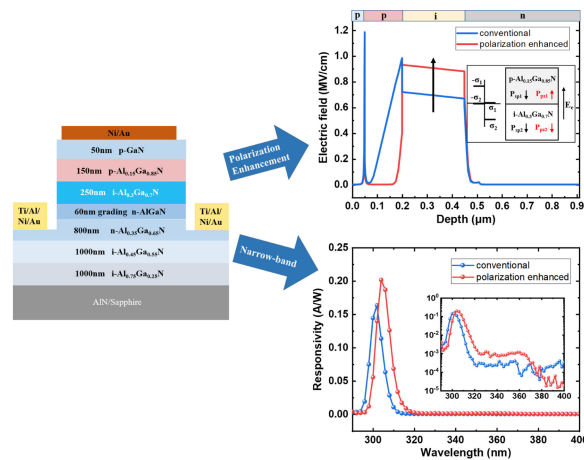


A High Quantum Efficiency Narrow-Band UV-B AlGaN p-i-n Photodiode With Polarization Assistance

Volume 13, Number 3, June 2021

Qianyu Hou
Haifan You
Qing Cai
Hui Guo
Pengfei Shao
Danfeng Pan
Le Yu
Dunjun Chen
Hai Lu
Rong Zhang
Youdou Zheng



DOI: 10.1109/JPHOT.2021.3086855

A High Quantum Efficiency Narrow-Band UV-B AlGaN p-i-n Photodiode With Polarization Assistance

Qianyu Hou , Haifan You , Qing Cai, Hui Guo, Pengfei Shao, Danfeng Pan, Le Yu, Dunjun Chen, Hai Lu , Rong Zhang, and Youdou Zheng

Key Laboratory of Advanced Photonic and Electronic Materials, School of Electronic Science and Engineering, Collaborative Innovation Center of Advanced Microstructures, Microfabrication and Integration Technology Center, Nanjing University, Nanjing 210093, China

DOI:10.1109/JPHOT.2021.3086855

This work is licensed under a Creative Commons Attribution 4.0 License. For more information, see <https://creativecommons.org/licenses/by/4.0/>

Manuscript received April 27, 2021; revised May 28, 2021; accepted June 2, 2021. Date of publication June 7, 2021; date of current version June 23, 2021. This work was supported in part by the National Natural Science Foundation of China (NSFC) under Grant 61634002, in part by the NSAF under Grant U1830109, in part by the Jiangsu Provincial Department of Water Resources, China under Grant 2019048, and in part by the Fundamental Research Funds for the Central Universities under Grant 021014380172. Corresponding author: Dunjun Chen (e-mail: djchen@nju.edu.cn).

Abstract: We designed and fabricated narrow-band UV-B AlGaN p-i-n photodiodes (PDs) with a full-width at half-maximum (FWHM) of 8 nm by optimizing the Al composition and thickness of the AlGaN layers. To improve the photoelectric response of the narrow-band PDs, a polarization electric field with the same direction with the applied bias field was introduced to the absorption layer by adjusting the Al composition ratio between the p-type AlGaN layer and i-type AlGaN absorption layer. The polarization enhanced narrow-band PD exhibited a higher external quantum efficiency (EQE) of 82% than the conventional one with an EQE of 67%. Meanwhile, a low dark current density of 1.7 nA/cm^2 and four orders of magnitude UV-visible rejection ratio were achieved for the enhanced narrow-band PDs with a maximum photocurrent responsivity of 202 mA/W at 304 nm.

Index Terms: AlGaN, narrow-band, photodiodes, polarization, responsivity, quantum efficiency.

1. Introduction

Ultraviolet photodiodes (PDs) have multitudes of military and civilian applications such as flame detection, astronomical studies, ozone monitoring, and ultraviolet imaging [1]–[6]. Compared with the photomultiplier tubes (PMT), which are bulky, fragile, and costly, photodiodes take advantage of filter-free and small size [7]. There are numerous types of reported UV PDs including Schottky-type, metal-semiconductor-metal, and p-i-n junction PDs [8]–[10]. Wide-bandgap AlGaN materials, which provide the photon wavelength range of 200–364 nm, have drawn increasing attention. AlGaN PDs are one of the most potential competitors for UV detection thanks to their outstanding optical and electrical properties, including low operating voltage and dark current density, high detectivity, excellent thermal stability, and radiation resistance [11]–[13].

For some special applications, such as phototherapy and identification of fluorescence, narrow-band PDs with small full-width at half-maximum (FWHM) and relatively high spectral selectivity are

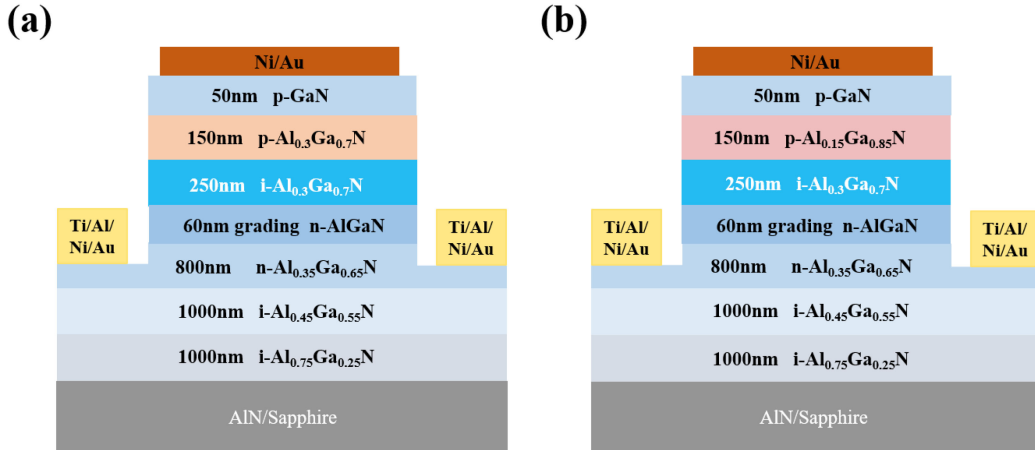


Fig. 1. The schematic cross-section of (a) the conventional and (b) the polarization enhanced narrow-band p-i-n AlGaN PD structures.

desirable [14]. Shao reported inorganic vacancy-ordered perovskite Cs₂SnCl₆:Bi/GaN narrow-band PDs with a FWHM of 18 nm for the spectral response, covering the spectral range of 360–400 nm [15]. B. Albrecht demonstrated a UV-B (280–315 nm) narrow-band AlGaN p-i-n PD with an EQE of 56% [16]. R. McClintock reported AlGaN-based PDs with a FWHM of 12.5 nm, and the maximum responsivity was 136 mA/W at 282 nm [17]. However, there still need more research about the design and optimization of AlGaN p-i-n photodiodes, especially for the UV-B narrow-band PDs with higher EQE for the detection and identification of specific fuel components.

In this work, we proposed and fabricated back-illuminated narrow-band UV-B AlGaN p-i-n PDs with a response window around 305 nm, which can realize the detection and identification of specific fuel components without using additional optical filters. This was achieved by adjusting the Al composition and the thickness of the AlGaN layers. In our proposed structure, a polarization electric field with the same direction with the applied bias field was introduced into the absorption layer by polarization engineering to improve the photoelectric response of the narrow-band AlGaN PDs. The structure parameters of the PDs were optimized by theoretical calculation, and the photoelectric properties of the fabricated narrow-band AlGaN PDs were characterized and analyzed.

2. Device Structure Design

2.1 Structure and Simulation Models

Fig. 1 shows the structure diagram of a conventional and a polarization enhanced AlGaN PDs. The polarization enhanced device consists of an unintentionally doped 1000-nm-thick Al_{0.75}Ga_{0.25}N buffer layer and an unintentionally doped 1000-nm-thick Al_{0.45}Ga_{0.55}N optical window layer, followed by an 800-nm-thick n-type Al_{0.35}Ga_{0.65}N Ohmic contact layer. To relieve the lattice mismatch we utilized a 60-nm-thick n-AlGaN layer with grading Al composition, followed by an unintentionally doped 250-nm-thick Al_{0.3}Ga_{0.7}N absorption layer, and a 150-nm-thick p-type Al_{0.15}Ga_{0.85}N layer. For better Ohmic contact we applied a 50-nm-thick p-type GaN layer. Except for the 150-nm-thick p-Al_{0.3}Ga_{0.7}N layer, the structure of conventional AlGaN PD was similar to the polarization enhanced counterpart. The hole concentration of the p-type AlGaN layers was $1 \times 10^{18} \text{ cm}^{-3}$.

ATLAS, a two-dimensional (2D) numerical device simulation tool based on Technology Computer Aided Design (TCAD), was performed to optimize the structure parameters. During the calculation, we utilized the models of Boltzmann, Standard Band-to-Band Tunneling, Concentration Dependent, Selberherr, and Shockley-Read-Hall Recombination. The polarization model was applied, which is crucial to AlGaN materials. Besides, there were several fundamental equations utilized in the

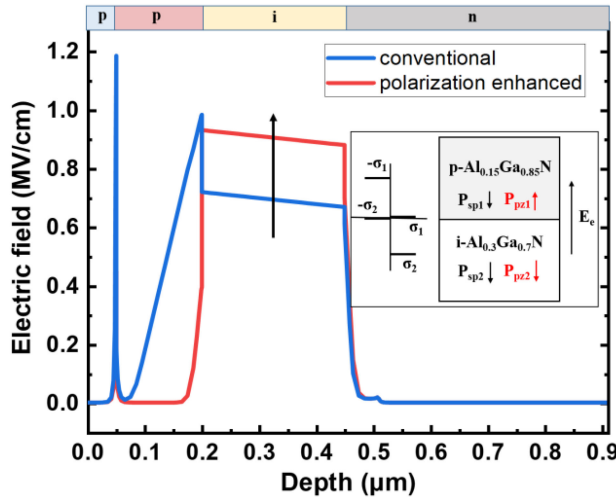


Fig. 2. Electric field distribution of the conventional and the enhanced p-i-n PDs at -20 V. Inset is the polarization electric field and charge distribution at the interface of the p-Al_{0.15}Ga_{0.85}N/i-Al_{0.3}Ga_{0.7}N layer.

simulation such as Poisson's Equation, the transport equations, and the continuity equations. And for the steady-state simulation, we utilized the Newton iteration method.

The refraction index and the absorption coefficient of GaN and Al_xGa_{1-x}N were extracted from [18]. The spectral responsivity of the PDs was calculated by

$$R = \frac{I_{\text{light}}}{P_{in}} = \frac{I_{\text{light}}}{BS}, \quad (1)$$

where R is the spectral responsivity, I_{light} is the light current, B is the intensity of the incident beam and S is the area of the incident light.

2.2 Simulation Results

Fig. 2 demonstrates the electric field distribution of the conventional and polarization enhanced AlGaN p-i-n PDs. For the polarization enhanced PD, the electric field spike has been mitigated at the junction of the p-AlGaN/i-Al_{0.3}Ga_{0.7}N layer, and electric field intensity in the p-type Al_{0.15}Ga_{0.85}N layer has dropped precipitously as compared with the conventional counterpart. This means that the width of the depletion region in the p-AlGaN layer is reduced by the introduction of polarization engineering. Hence, the out-of-band photo-generated current caused by the p-Al_{0.15}Ga_{0.85}N layer will decrease. This is beneficial to achieve a higher in/out-of-band responsivity rejection ratio. Moreover, the electric field intensity of the enhanced PD in the absorption layer has increased by 32% as compared with the conventional counterpart, which is conducive to the separation and extraction of photo-generated carriers.

The distribution of polarization electric field and bound charge are shown in the inset of Fig. 2. To clarify the polarization effect in detail, we calculated the total polarization sheet charge at the junction of the p-Al_{0.15}Ga_{0.85}N/i-Al_{0.3}Ga_{0.7}N layer. The polarization sheet charge σ (σ_1 and σ_2) is defined as the sum of bound charges generated by the piezoelectric polarization and spontaneous polarization. The charge σ_1 and σ_2 are originated from the p-Al_{0.15}Ga_{0.85}N layer and the i-Al_{0.3}Ga_{0.7}N layer, respectively. And the calculated value of σ_1 is 1.06×10^{13} C/cm² whereas σ_2 is 1.32×10^{13} C/cm². Thus, a negative polarization charge of 2.6×10^{12} C/cm² is introduced to the upper surface of the absorption layer. Similarly, a positive polarization charge of 0.2×10^{12} C/cm² is introduced at the junction of i-Al_{0.3}Ga_{0.7}N/n-AlGaN by calculation. A polarization electric field with the same direction with the applied bias field is introduced to the absorption

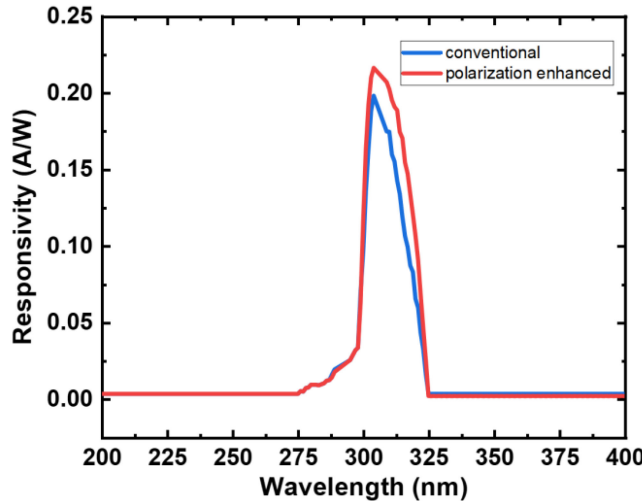


Fig. 3. Spectral response characteristics of the conventional and enhanced PDs under the applied bias of -20 V by simulation.

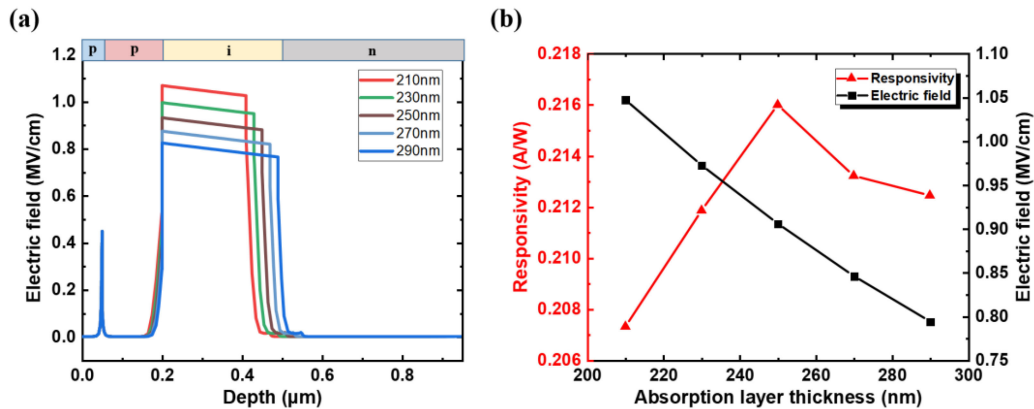


Fig. 4. (a) Electric field distribution with different thicknesses of the absorption layer. (b) Maximum responsivity and the average electric field intensity in the i-Al_{0.3}Ga_{0.7}N absorption layer versus the absorption layer thickness of the enhanced AlGaN PD at -20 V.

layer through introducing polarization enhanced Al_{0.15}Ga_{0.85}N/Al_{0.3}Ga_{0.7}N heterostructure. This accounts for the enhancement of the electric field in the absorption layer.

The spectral responses of the back-illuminated AlGaN PDs are displayed in Fig. 3. The polarization enhanced PD shows a responsivity of 216 mA/W, which is 9% higher than the conventional counterpart. The improvement of spectral responsivity can be explained by the enhancement of the electric field intensity in the absorption layer.

The number of photogenerated carriers and the electric field intensity are the key factors for the responsivity. And the thickness of the absorption layer greatly affects the number of photogenerated carriers and the electric field intensity. Then we investigated the optimum thickness of the i-Al_{0.3}Ga_{0.7}N layer in the polarization enhanced AlGaN p-i-n PDs. As displayed in Fig. 4(a), with the decrease of the thickness in the i-Al_{0.3}Ga_{0.7}N absorption layer, the electric field intensity increases gradually. To demonstrate the influence of thickness on devices performance preferably, the thickness-dependent maximum responsivity and the average electric field intensity in the absorption layer are demonstrated in Fig. 4(b), respectively. We observed that reducing the thickness of the i-Al_{0.3}Ga_{0.7}N absorption layer can increase the electric field intensity. And

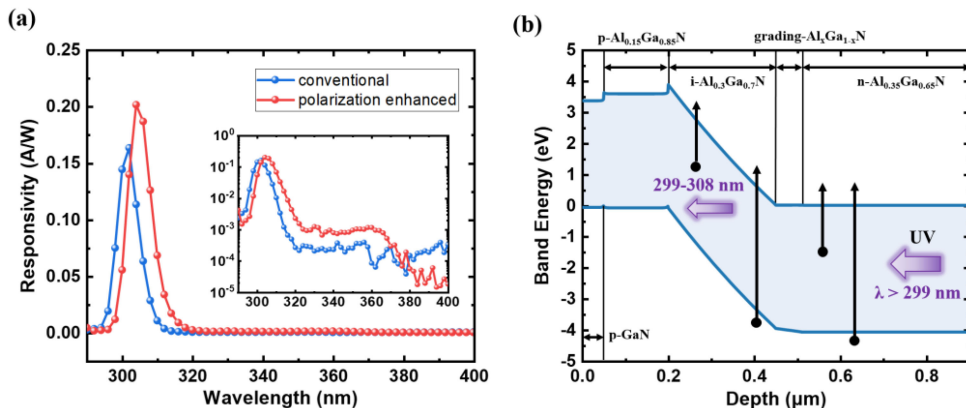


Fig. 5. (a) Spectral response characteristics of the fabricated conventional and enhanced AlGaN PDs with a mesa area of $6362 \mu\text{m}^2$ at -20 V. Inset is a log plot of the spectral responsivity. (b) Energy band of the polarization enhanced PD at 0 V.

excessive thin thickness of the i-AlGaN absorption layer will affect the absorption of photons, thus resulting in a lower photocurrent. Therefore, as demonstrated in Fig. 4(b), with the reduction of the absorption thickness, the maximum responsivity shows a trend of rising first and then declining. The responsivity achieves the maximum value when the thickness of the absorption layer is 250 nm.

3. Device Fabrication

3.1 Fabrication

The device structures illustrated in the simulation section were grown on AlN templates with double-side polished sapphire substrates by utilizing a metal-organic chemical vapor deposition system. Photolithography and dry etching using the gas of Cl₂/BCl₃ (30/8 sccm) were applied to fabricate the 90-μm-diameter mesa structure. The mesa etching left a 400-nm-thick n-type Al_{0.35}Ga_{0.65}N to reduce the short-wavelength out-of-band absorption. Then Ti/Al/Ni/Au (20/140/60/160 nm) was deposited on the n-type Al_{0.35}Ga_{0.65}N layer, and the device was rapidly annealed at 850°C for 30s in N₂ ambient to form Ohmic contact. Finally, a thin 40-μm-diameter Ni/Au (20/20 nm) layer was evaporated and annealed at 550°C for 12 min in air ambient for p-type Ohmic contact. The fabricated PDs were characterized using a 6-mm-diameter UV fiber and a probe station. A Xeon lamp was utilized as the incident light source and a reference Si detector was applied to calibrate.

3.2 Results and Discussions

Fig. 5(a) shows the spectral response of the conventional and polarization enhanced UV-B narrow-band AlGaN p-i-n PDs at the applied bias of -20 V. Similarly, both devices exhibit excellent performance with a narrow response band and a comparatively steep band cut-off. The conventional AlGaN PD has a peak value responsivity of 163 mA/W at 302 nm whereas the maximum responsivity of the polarization enhanced PD reaches a value of 202 mA/W at 304 nm. The external quantum efficiency (EQE) has increased from 67% to 82%. The significant improvement in EQE and responsivity is due to the adjustment of the Al composition in the p-type AlGaN layer by polarization engineering. This leads to the enhancement of the electric field intensity. In this way, the photo-generated carriers can be separated more quickly in the depletion region, resulting in higher photocurrent. A log plot of the spectral responsivity is displayed in the inset of Fig. 5(a). The photocurrent response of the polarization enhanced PD is stronger than the conventional

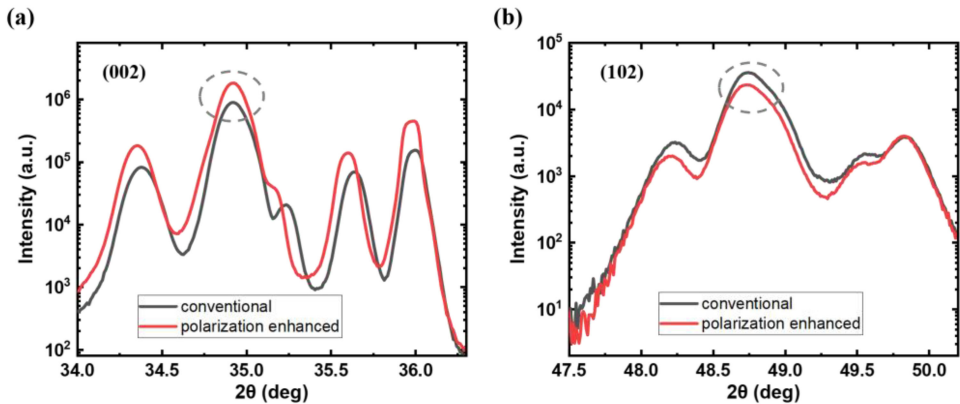


Fig. 6. (a) (002) and (b) (102) ω - 2θ scan of the conventional and enhanced PDs.

counterpart around 305-380 nm. This can be attributed to the increase of the electric field intensity by polarization engineering. Besides, the spectral response of the enhanced device around 330 nm is caused by the absorption of photons in the p-Al_{0.15}Ga_{0.85}N layer [19]. When the incident wavelength is higher than 380 nm, the spectral responsivity is about one order of magnitude lower than the conventional counterpart. It indicates that the polarization enhanced PD has a higher UV (304 nm)-visible (400 nm) rejection ratio, exceeding 10⁴.

The spectral responsivity curve of the polarization enhanced PD also demonstrates a narrow waveform with a rapidly rising band edge at 299 nm, a cut-off band tendency at 305 nm, as well as a relatively small FWHM of 8 nm, indicating an outstanding UV-B detecting ability and an excellent bandpass capability. The excellent spectral performance benefits from the design of the optical window structure. The light absorption outside the depletion region contributes little to the photocurrent. When light is incident from the back of the device, the ultraviolet light with wavelength less than 280 nm is difficult to reach the depletion region since it has been completely absorbed by the 1000-nm-thick Al_{0.45}Ga_{0.55}N window layer. And a 400-nm-thick n-type Al_{0.35}Ga_{0.65}N layer was left to absorb 280-299 nm ultraviolet light during the etching process. Therefore, as shown in Fig. 5(b), what is of great significance to the photocurrent is the light with a wavelength longer than 299 nm. The steep cut-off band edge is attributed to the low defects in the i-Al_{0.3}Ga_{0.7}N absorption layer, which has an absorption wavelength about 308 nm.

The response of the polarization-enhanced device is found to be red-shifted about 2 nm as compared with the conventional counterpart. One possible reason for the redshift may be the light absorption in the p-Al_{0.15}Ga_{0.85}N layer. Besides, the deviation of Al composition in the growth process of these two devices may be another cause of the red-shift. Fig. 6 shows (002) and (102) ω - 2θ scan of the conventional and enhanced PDs. We focus on the Al composition of the i-AlGaN layers. Through calculation, the Al composition of the i-AlGaN layer for the conventional PD is estimated to be 32.5% and the Al composition of the i-AlGaN layer for the enhanced PD is 32.3%. The calculation result is consistent with the result of the spectral response.

Meanwhile, a table shows the excellent performance of the polarization-enhanced PD compared with other published detectors (Table 1). The enhanced PD in this work exhibits higher EQE and smaller FWHM.

The room-temperature current-bias characteristics were measured under dark and ultraviolet illumination conditions utilizing a cascade probe station and a Keithley 4200 analyzer. Fig. 7 presents the reverse-biased I-V curves of a polarization-enhanced device with a mesa area of 6362 μm^2 . With the increase of reverse voltage, the dark current keeps a low value below 1 pA while the photocurrent keeps a slowly rising, strong response. The leakage current density shows a low value of 1.7 nA/cm² at -1 V and increases to 8.6 nA/cm² at -20 V. The low dark current indicates high-quality junction interfaces of the enhanced PD [27].

TABLE 1
Detector Performance Compared With Other Detectors

PD Structure	λ^a (nm)	η_{\max}^b (%)	FWHM ^c (nm)	Reference
GaN-based	378	68.1% (-15 V)	18	[15]
p-i-n	310	56% (0 V)	47	[16]
p-i-n	282	72% (-5 V)	12.5	[17]
MSM	240	-	46	[20]
p-i-n	278	23% (-20V)	12	[21]
p-i-n	245	80% (-10 V)	41	[22]
p-i-n	289	45.5% (0 V)	27	[23]
p-i-n-i-n	290	67.4% (0 V)	9	[24]
p-i-n	280	42% (-40 V)	33	[25]
MIS	270	70.6% (-3 V)	12	[26]
p-i-n	304	82% (-20 V)	8	This work

^aPeak detection wavelength of the detector.

^bMaximum quantum efficiency at the peak wavelength.

^cFull-width at half-maximum of spectral response.

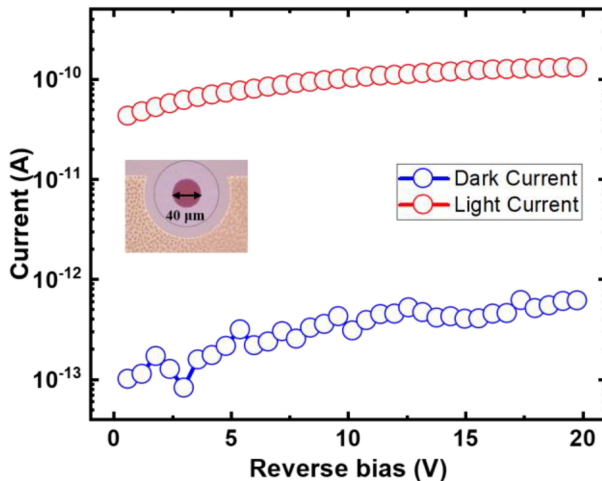


Fig. 7. Reverse-biased I-V diagram of a polarization enhanced device (anode diameter: 40 μm) with a mesa area of 6362 μm^2 under dark and UV light conditions.

4. Conclusion

In summary, back-illuminated polarization-enhanced narrow-band UV-B AlGaN p-i-n PDs with high EQE were achieved. A negative polarization sheet charge of $2.6 \times 10^{12} \text{ C/cm}^2$ was introduced at the interface of the p-Al_{0.15}Ga_{0.85}N/i-Al_{0.3}Ga_{0.7}N layer. This resulted in a higher value of electric field intensity in the i-AlGaN absorption layer along with a preferable spectral responsivity compared to the conventional devices. For the fabricated enhanced narrow-band PD with a FWHM of 8 nm, covering the spectral range of 298–316 nm, the measured spectral responsivity was up to 202 mA/W at 304 nm. The corresponding EQE was 82%. The UV (304 nm)-to-visible (400 nm) rejection ratio exceeded 10⁴. Moreover, the dark current density was 1.7 nA/cm² under the reverse bias of 1 V, increasing to 8.6 nA/cm² at -20 V.

References

- [1] E. Monroy, F. Omnes, and F. Calle, "Wide-bandgap semiconductor ultraviolet photodetectors," *Semicond. Sci. Technol.*, vol. 18, no. 4, pp. R33–R51, Apr. 2003.
- [2] S. J. Pearton *et al.*, "GaN-based diodes and transistors for chemical, gas, biological and pressure sensing," *J. Phys.: Condens. Matter*, vol. 16, no. 29, pp. R961–R994, Jul. 2004.
- [3] W. Z. Xu *et al.*, "Magnesium ion-implantation-based gallium nitride p-i-n photodiode for visible-blind ultraviolet detection," *Photon. Res.*, vol. 7, no. 8, pp. B48–B54, Aug. 2019.
- [4] Q. Cai *et al.*, "AlGaN ultraviolet avalanche photodiodes based on a triple-mesa structure," *Appl. Phys. Lett.*, vol. 113, no. 12, Sep. 2018, Art. no. 123503.
- [5] M. Razeghi and A. Rogalski, "Semiconductor ultraviolet detectors," *J. Appl. Phys.*, vol. 79, no. 10, pp. 7433–7473, May. 1996.
- [6] J. Wang *et al.*, "Do all screw dislocations cause leakage in gan-based devices?," *Appl. Phys. Lett.*, vol. 116, no. 6, Feb. 2020, Art. no. 062104.
- [7] Y. Zhang *et al.*, "Low-noise GaN ultraviolet p-i-n photodiodes on GaN substrates," *Appl. Phys. Lett.*, vol. 94, no. 22, Jun. 2009, Art. no. 221109.
- [8] N. Biyikli, I. Kimukin, O. Aytur, and E. Ozbay, "Solar-blind AlGaN-based p-i-n photodiodes with low dark current and high detectivity," *IEEE Photon. Technol. Lett.*, vol. 16, no. 7, pp. 1718–1720, Jul. 2004.
- [9] J. Y. Duboz, N. Grandjean, F. Omnes, M. Mosca, and J. L. Reverchon, "Internal photoemission in solar blind AlGaN schottky barrier photodiodes," *Appl. Phys. Lett.*, vol. 86, no. 6, Feb. 2005, Art. no. 063511.
- [10] B. Yang *et al.*, "High-performance back-illuminated solar-blind AlGaN metal-semiconductor-metal photodetectors," *Electron. Lett.*, vol. 36, no. 22, pp. 1866–1867, Oct. 2000.
- [11] Z. Alaie, S. M. Nejad, and M. H. Yousefi, "Recent advances in ultraviolet photodetectors," *Mater. Sci. Semicond. Process.*, vol. 29, pp. 16–55, Jan. 2015.
- [12] C. J. Collins *et al.*, "Improved solar-blind detectivity using an $\text{Al}_x\text{Ga}_{1-x}\text{N}$ heterojunction p-i-n photodiode," *Appl. Phys. Lett.*, vol. 80, no. 20, pp. 3754–3756, May. 2002.
- [13] D. B. Li, K. Jiang, X. J. Sun, and C. L. Guo, "AlGaN photonics: Recent advances in materials and ultraviolet devices," *Adv. Opt. Photon.*, vol. 10, no. 1, pp. 43–110, Mar. 2018.
- [14] S. Rajamani *et al.*, "Deep UV narrow-band photodetector based on ion beam synthesized indium oxide quantum dots in Al_2O_3 matrix," *Nanotechnology*, vol. 29, no. 30, Jul. 2018, Art. no. 305603.
- [15] D. L. Shao, W. G. Zhu, G. Q. Xin, J. Lian, and S. Sawyer, "Inorganic vacancy-ordered perovskite $\text{Cs}_2\text{SnCl}_6:\text{Bi}/\text{GaN}$ heterojunction photodiode for narrowband, visible-blind UV detection," *Appl. Phys. Lett.*, vol. 115, no. 12, Sep. 2019, Art. no. 121106.
- [16] B. Albrecht *et al.*, "Improved AlGaN p-i-n photodetectors for monitoring of ultraviolet radiation," *IEEE J. Sel. Topics Quantum Electron.*, vol. 20, no. 6, Nov./Dec. 2014, Art. no. 3802507.
- [17] R. McClintock *et al.*, "High quantum efficiency AlGaN solar-blind p-i-n photodiodes," *Appl. Phys. Lett.*, vol. 84, no. 8, pp. 1248–1250, Feb. 2004.
- [18] J. F. Muth *et al.*, "Absorption coefficient and refractive index of GaN, AlN and AlGaN alloys," *MRS Internet J. Nitride Semicond. Res.*, vol. 4S1, 1999, Art. no. G5.2.
- [19] X. Z. Dang, C. D. Wang, E. T. Yu, K. S. Boutros, and J. M. Redwing, "Persistent photoconductivity and defect levels in n-type AlGaN/GaN heterostructures," *Appl. Phys. Lett.*, vol. 72, no. 21, pp. 2745–2747, May. 1998.
- [20] S. V. Averin *et al.*, "AlN/AlGaN heterostructures for selective ultraviolet MSM detectors," *Tech. Phys.*, vol. 56, no. 2, pp. 295–297, Feb. 2011.
- [21] D. J. H. Lambert *et al.*, "Back illuminated AlGaN solar-blind photodetectors," *Appl. Phys. Lett.*, vol. 77, no. 12, pp. 1900–1902, Sep. 2000.
- [22] T. T. T. Pham, J. H. Choi, C. H. Cho, and H. Y. Cha, "Filter-free AlGaN photodiode with high quantum efficiency for partial discharge detection," *J. Semicond. Technol. Sci.*, vol. 20, no. 2, pp. 141–144, Apr. 2020.
- [23] A. Kalra, S. Rathkanthiwar, R. Muralidharan, S. Raghavan, and D. N. Nath, "Material-to-device performance correlation for AlGaN-based solar-blind p-i-n photodiodes," *Semicond. Sci. Technol.*, vol. 35, no. 3, Mar. 2020, Art. no. 035001.
- [24] Y. R. Chen, Z. W. Zhang, Z. M. Li, H. Jiang, G. Q. Miao, and H. Song, "The influence of n-AlGaN inserted layer on the performance of back-illuminated AlGaN-based p-i-n ultraviolet photodetectors," *Phys. Status Solidi A-Appl. Mat.*, vol. 215, no. 2, Jan. 2018, Art. no. 1700358.
- [25] T. Tut, T. Yelboga, E. Ulker, and E. Ozbay, "Solar-blind AlGaN-based p-i-n photodetectors with high breakdown voltage and detectivity," *Appl. Phys. Lett.*, vol. 92, no. 10, Mar. 2008, Art. no. 103502.
- [26] W. Y. Han *et al.*, "High performance back-illuminated MIS structure AlGaN solar-blind ultraviolet photodiodes," *J. Mater. Sci.-Mater. Electron.*, vol. 29, no. 11, pp. 9077–9082, Jun. 2018.
- [27] C. J. Collins *et al.*, "Improved device performance using a semi-transparent p-contact AlGaN/GaN heterojunction positive-intrinsic-negative photodiode," *Appl. Phys. Lett.*, vol. 75, no. 14, pp. 2138–2140, Oct. 1999.